Experimental and numerical evaluation of hydro-thermal ageing's effects on adhesive connections in offshore structures

Marco Lamberti, Aurélien Maurel-Pantel, Frédéric Lebon

Experimental and numerical evaluation of hygro-thermal ageing's effects on adhesive composite connections in offshore structures

Marco Lamberti [1-2,*], Aurelien Maurel-Pantel[2], Frederic Lebon[2]

[1] ENEA, Brasimone Research Center, Italy
[2] Aix-Marseille University, CNRS, Centrale Marseille, LMA, Marseille, France

* *corresponding author*

Abstract

In offshore structures born over time the need to replace or reinforce existing metal members. A possible solution is represented by using bonded connections. In this paper, a simple and efficient semi-analytical procedure is developed to design or verify existing structures reinforced by bonding steel elements. The model can evaluate the interfacial shear stress at all loading stages up to the failure of adhesive connections exposed in the marine environment. The metal adherents bonded together can undergo slip at the interface. The model is based on Bernoulli beam theory and satisfies the requirements of equilibrium and strain compatibility allowing for interfacial deformations. The adherents are treated as non-linear material with an elastoplastic strain hardening behaviour. The adhesive layer takes into account the degradation process under ageing conditions. The presented formulation has been validated employing a finite element model.
In addition, double lap shear and end-notched flexural experimental tests have been performed to evaluate the cohesive behaviour in mode II of polyurethane structural adhesive under the combined effects of water and temperature during 150 days of exposure. The experimental results have been implemented in the numerical procedure. The numerical analyses show that the adhesive connections' performance is influenced by the short ageing conditions.

Keywords: Hygro-thermal behaviour, semi-analitycal model, adhesive connection, short ageing

1. Introduction

The use of adhesive for realizing structural joints in mechanical and civil engineering is spreading more such as by co-bonding or secondary bonding [1].
One of the most important characteristics of adhesive connections is the possibility of joining dissimilar materials such as steel, aluminium, and fibre-reinforced composites.
Furthermore, the speed of installation or replacement of structural elements and the facility of maintenance and the improvement of corrosion [2], features needful in marine applications, lead to consider these type's connections particularly suitable for the construction of secondary members such as the wind installations in the offshore structures [3]-[5].
As is well known, the damage mechanisms of adhesive connections can be influenced by various factors such as loading conditions, mechanical properties of adhesive and adherents, adhesive thickness, and adhesion quality. Among them, the presence of leading causes of degradation, such as ageing, is an aspect to be deeply investigated.
Therefore, a deep and complete understanding of the behaviour of adhesive joints in ageing environments becomes fundamental to exploiting their capabilities in civil and mechanical applications.
Indeed, there are different types of adhesives capable of being used in structural applications. Beyond the already extended use of epoxy adhesives, polyurethane based adhesives are started to be used increasingly more [6]. In fact, polyurethanes are being implemented in the industry in different ways mainly thanks to their good properties against external agents [7] after recent studies have shown the capability of this material to be used in structural applications [8]-[11].
Adhesive durability and joint reliability are key parameters still under evaluation that strongly affect the performance of adhesive joints over time in both civil and mechanical engineering fields [12].
Some research works, focused on the investigation of the effects of humidity and temperature on the mechanical performance of adhesive joints, can be found in the literature, indeed in most cases are related to the use of epoxy adhesives [13]-[15]. Viana et al. [16] developed a review about the degradation of adhesive joints caused by temperature and humidity applications. The influence of severe environment on the resistance in terms of shear and tensile strength of multi-material adhesive joints has been studied in [17], as well as the effect of combined environmental loads on the behaviour of metal-composite adhesive joints [18]. Costa et al. [19] studied the fatigue behaviour of aluminium adhesive joints after water immersion. Heshmati et al. [20] found a direct relationship between moisture content and mechanical properties degradation by analysing the effect of moisture on the performance of an epoxy adhesive. Indeed, is not possible to extend this relationship in the case of polyurethane adhesives.
Ageing mechanisms of polyurethane adhesives are studied in the literature [21]-[22], but still need to investigate the study of mechanical behaviour of polyurethane joints under the combined effect of temperature and water.
Furthermore, to design and verify the adhesive connections, it is crucial to know the mechanical properties of adhesives such as strength and fracture energy but also their durability [23].
Nowadays, few experimental data about adhesive fracture energy are available in the literature making the use of bonded joints, especially in the field of mechanical and civil engineering, a hard challenge [24]-[26].

Some researchers focused their studies on the evaluation of the influence of the temperature on the fracture energy [27]-[29], on the other hand others analysed the performance and/or durability of adhesive joints in the presence of temperature and moisture with adherents made of carbon [30]-[31], glass and [32] and steel [33]-[35].

Indeed, a complete evaluation of the behaviour of polyurethane adhesive under the combined effect of water and temperature is still lacking. The importance to define the mechanical mechanism at the interface of adhesive under the aging condition in the design of structural application covered an aspect of primary importance.

In literature, the most common approach for the numerical modelling of adhesives is the macroscopic model named cohesive zone defined by a traction separation law used for large-scale analysis thanks to the low computational cost and its simplicity [36]-[37]. The cohesive zone model can capture the phenomena typically observed in structural adhesive applications such as crack propagation.

Although the cohesive model is widely validated for structural epoxy-based adhesives, Dasai et al. [38] found experimentally a traction separation law for polyurethane adhesive through double cantilever beam tests.

In this framework, to design and verify new bonded connections or repaired structures made by steel adherents, the fracture energies considering the effect of ageing conditions on the relative interface law represent a crucial parameter to know.

To define the interface law in Mode II and the degradation effect of short ageing conditions due to the application of the combined effect of temperature and water some experimental tests have been undertaken and the main results analysed.

More in detail, double lap shear and End Notch Failure (ENF) tests have been performed to define the interface parameters such as shear strength and fracture energy in mode II. The specimens were placed in water at 60°C utilizing an oven and tested during a time of 150 days. The experimental results have been permitted to identify the cohesive law in mode II.

Furthermore, an efficient semi-analytical procedure is proposed by authors who intend to study the influence of hygro-thermal ageing on the mechanical behaviour of adhesive joints with polyurethane adhesive. The model is based on the Bernoulli beam theory and satisfies the requirements of equilibrium and strain compatibility allowing for interfacial deformations. The adherents are treated as non-linear material with an elastoplastic strain hardening behaviour. The governing equations are formulated as two second-order differential equations with their dependent variables. The equations are solved for discrete states experienced by the steel adherents and their associated level of interfacial slip. The presented formulation has been validated employing a finite element model.

The analytical model permit to design of safe structural adhesive steel joints considering the effect of ageing on the adhesive layer. In fact, the analytical model is based on the hypothesis that the degradation phenomena due to the ageing conditions occur only in the adhesive layer, being the adherents of a metallic nature.

2. Analytical formulation

Let Fig. 1 represents some examples of composite structures made by steel elements bonding together using a structural adhesive. More in detail, the composite structure shown in Figure 1 (a) is composed of a HE steel profile reinforced with a steel plate. Another example is shown in Fig. 1 (b), where a horizontal plate is bonded on two square columns and ended with a rectangular plate in order to realize a railing.
These types of structural applications can be thought of for secondary structures in offshore wind installations. It is important to underline that the use of bonded connections avoids the dangers and the slag deriving from welding operations in the marine environment.

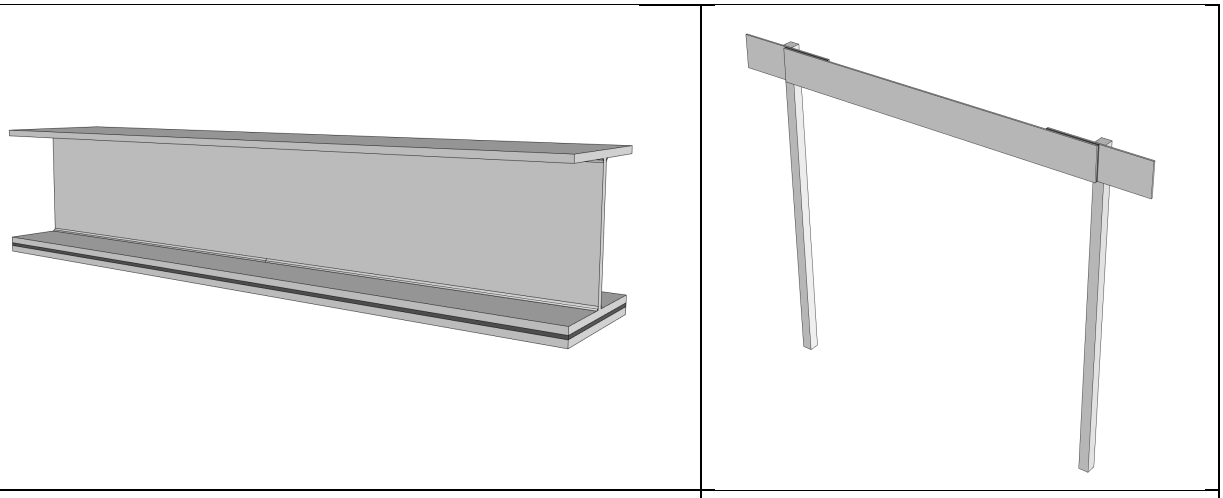

(a) **(b)**

Fig. 1 – 3D view of composite adhesive structures

The composite structure is subjected to uniformly distributed load *q* as depicted in Figure 2.
In this figure, *Lq* denotes the length of the element subject to a uniformly distributed load. Due to symmetry only half of the composite structure is considered in the development of analytical formulation.
Notice, the proposed methodology is not theoretically limited to symmetrically or uniformly loaded, but these are imposed in the current investigation.

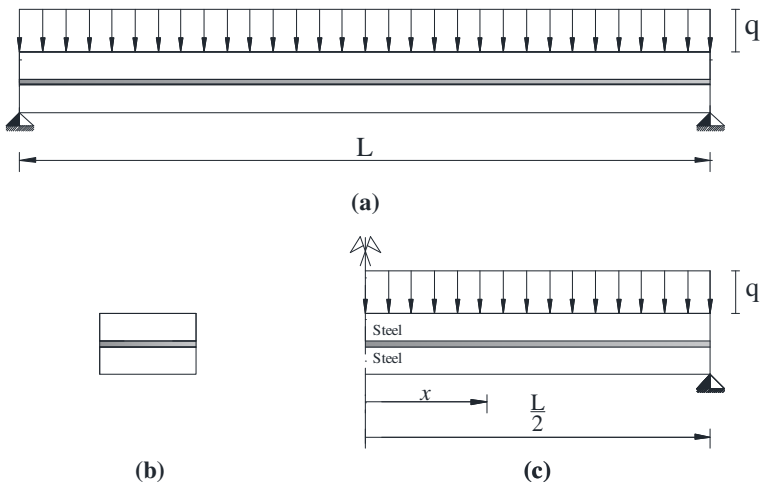

Figure 2: Composite beam analyzed.

In Figure 3, the cross-section of the steel adhesive connections, subjected to the external moment due to the load applied, is depicted. Note that F_{S1} and M_{S1} are the force and moment resultants of the stresses in the upper steel profile acting through the centroid while F_{S2} and M_{S2} are the force and moment resultants of the stresses in the lower steel profile. Finally, Fa represents the longitudinal force due to the presence of the adhesive layer.
To satisfy equilibrium, F_{S1} compression force in the upper steel horizontal plate must be equal to F_{s2}, the tensile force in the lower steel profile.

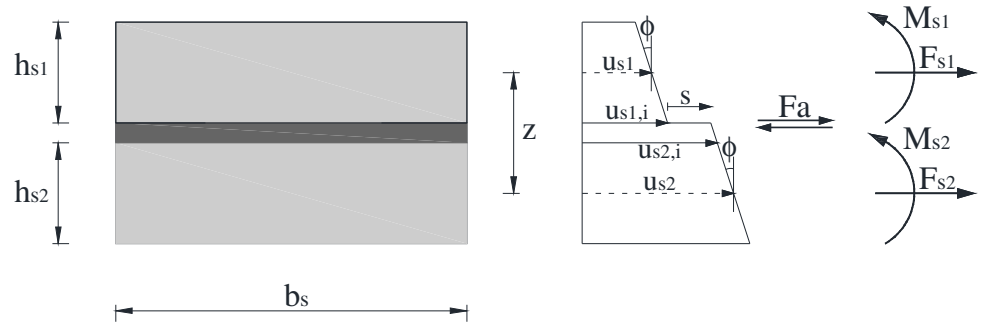

Figure 3: Transverse section of the steel-concrete composite beam.

Furthermore, u_{S1} and u_{s2} represent the centroidal axial displacement of the upper and lower section, respectively. Observe, the slip λ at the interface can be expressed as

$$\lambda = u_{S1,i} - u_{S2,i} = u_{S1} - u_{S2} + \phi z \quad (1)$$

where $u_{s1,i}$ and $u_{s2,i}$, represent the axial displacement of the upper and lower steel member at their interface, respectively, ϕ the section rotation and z the distance between the centroids of the respective section. In the present formulation, the steel profiles are assumed to have equal vertical displacement and rotation at any section according to the Bernoulli beam theory.
Considering the moment equilibrium of the composite cross section, the external moment, M_e, due to the applied load acting on the steel adhesive connection, is equilibrated at any section by the sum of the resisting moment of the upper member, M_{S1}, and the resisting moment of the lower member, M_{S2}, plus the moments generated by the presence of axial forces, as expressed in Eq. (2):

$$M_e = M_{S1} + M_{S2} + F_{S2} d_{S2} - F_{S1} d_{S1} = M_{S1} + M_{S2} + F_a d_S \quad (2)$$

Moreover, from equilibrium of internal axial forces:

$$F_{S2} = -F_{S1} = F_a \quad (3)$$

The moment arms, d_{s1} and d_{s2} in Eq. (2) represent the distance between the interface and the centroid of the upper and lower steel elements, respectively.

It is important to point out that from the equilibrium of the horizontal forces acting on the steel profile elements in Fig. 2, the interfacial shear flow is given by

$\frac{dF_a}{dx} = -\tau b$	(4)

where τ is the interfacial shear stress at the interface of the adhesive layer. In the current model the origin of the coordinate x is located at midspan. The interfacial shear stress is a function of the slip λ at the adhesive interface.

The moment of the steel profile can be related to the section curvature χ. Non-linear behaviour can be captured considering the non-linearity of its components.
The non-linear $M_S - \chi$ response can be approximated as a bilinear curve as well as the resultant force-extreme fiber steel strain (Nj-ε) diagrams for a steel profile, depicted in Fig. 4(b).
In the figure, the moments M_{Sy} and M_{Su}, respectively, represent the yielding and ultimate moment and denote the corresponding curvatures.

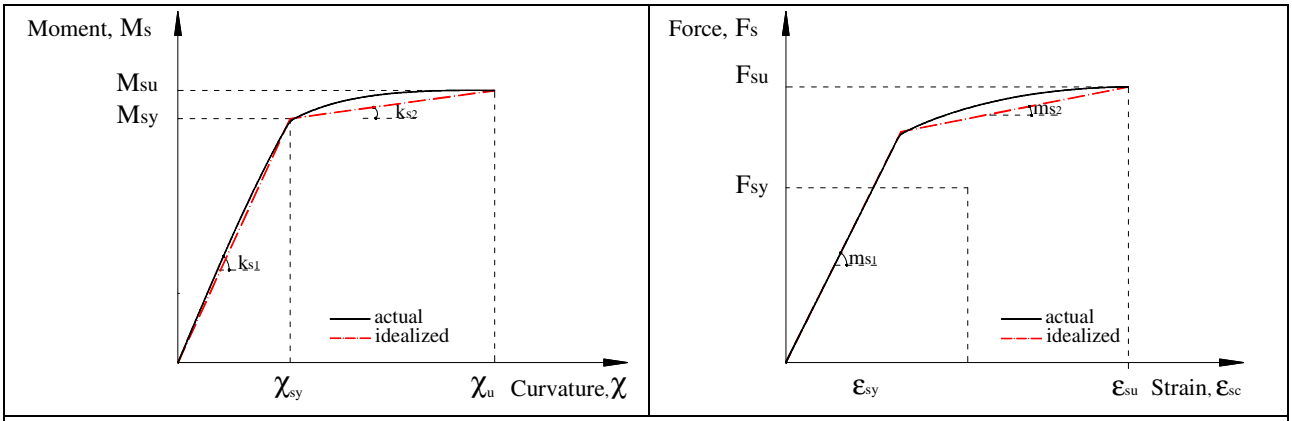

Figure 4: (a) Bilinear moment-curvature curve for steel section
(b) Bilinear Steel section resultant compression force-strain curve

The metal constitutive relationship is here reported:

$M_j = \chi E_{i,j} I_{i,j}$	(5a)
$M_j = M_{y,j} + E_{i,j} I_{i,j} \left(\chi - \chi_{y,j} \right)$	(5b)

i= 1,2 first and second branch, j=1,2 first and second steel adherent.

$N_j = \sigma_j A_j = \varepsilon_j E_i A_j$	(6a)
$N_j = N_{y,j} + E_i A_j \left(\varepsilon - \varepsilon_{y,j} \right)$	(6b)

By satisfying the compatibility (Eq. 1) and equilibrium (Eq. 3) requirements, and by using the constitutive relations (Eq. 6), it can be obtained the expression of the slip's derivative function of curvature:

$$\frac{d\lambda}{dx} = -F_a\mu^* + n^* + \chi d_s \quad (7)$$

with

$$\mu^* = \left(\frac{E_{1,j}A_{1,j} + E_{2,j}A_{2,j}}{E_{1,j}A_{1,j}E_{2,j}A_{2,j}} \right) \quad (8a)$$

$$n^* = \frac{N_{y,2} - \varepsilon_{y,2}E_{y,2}A_{2,j}}{E_{2,j}A_{2,j}} - \frac{N_{y,1} - \varepsilon_{y,1}E_{y,1}A_{1,j}}{E_{1,j}A_{1,j}} \quad (8b)$$

Considering the equilibrium (Eq. 2-3) and by using the constitutive relations (Eq. 6), the expression of curvature has been calculated:

$$\chi = \left(\frac{M_e - m^*}{d_S} - F_a \right) k^* \quad (9)$$

where

$$m^* = \frac{M_{y,1} + M_{y,2} - \left(E_{1,j}I_{1,j}\chi_{y,1} + E_{2,j}I_{2,j}\chi_{y,2} \right)}{E_{1,j}I_{1,j} + E_{2,j}I_{2,j}} \quad (10a)$$

$$k^* = \frac{d_S}{E_{1,j}I_{1,j} + E_{2,j}I_{2,j}} \quad (10b)$$

Substituting the expression of curvature (Eq.9) in Eq.7, the following expression has been calculated:

$$\frac{d\lambda}{dx} = -F_a\left(\mu^* + k^* d_S \right) + \left(M_e + m^* \right) k^* - n^* \quad (11)$$

2.1 *Adhesive interfacial slip law*

Over time, the bonded connections are subjected to a degradation process of the adhesive mechanical properties due to the presence of external environmental conditions especially in the case of marine applications. In fact, in the case of metal adherents bonding together, the weak element which may be subject to a rapid ageing process, is doubtless the adhesive layer. Moreover, seawater environments can be provoking reversible or permanent changes on the mechanical properties at longer ageing times to the adhesive, and to the substrate/adhesive interface.
In the current analytical investigation, the adhesive layer is considered subject to a degradation process with respect the metal elements whose mechanical properties are invariant over time.
To take into account the change of adhesive properties at the interface, the approach of Liu et al. [1] can be considered. The cohesive properties such as the shear stress, stiffness and fracture energies can be reduced depending on the environmental condition, as depicted in Figure 5.
In this approach, a simple assumption was made: the properties of the adhesive are degraded by multiplying an estimated factor according to the environmental conditions as reported in Eq. 12.

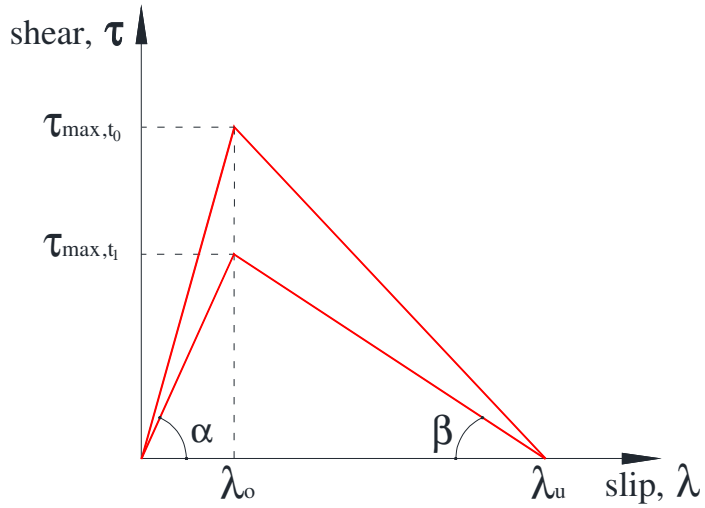

Figure 5: Interfacial shear slip law.

$\tau^h = c_1 \tau_0^{c_2}$	(12a)
$G^h = c_3 G_0^{c_4}$	(12b)

where τ^h and τ_0 are maximum shear stress with and without ageing; G^h and G_0 are fracture energy of adhesive with and without ageing, which can be obtained from experimental tests, and c_i (i=1 to 4) are extra degrading factors. The degrading factors were estimated by experimental tests in ageing conditions.
For the sake of simplicity, the non-linear behaviour of the interface can be idealized by a bilinear elastic-softening relationship as shown in Eq. (13).

$\tau^h = \alpha\lambda \quad \text{for } \lambda < \lambda_0$	(12a)

$\tau^h = \beta(\lambda_u - \lambda)$ for $\lambda_0 < \lambda < \lambda_u$	(12b)

By satisfying the compatibility (Eq. 1) and equilibrium (Eq. 2-3) requirements, and by using the interface shear-slip relationship (Eq. 4) and the constitutive relations (Eq. 5-6), the solution of the governing equations can be obtained, depending on the evolution of interfacial slip and the state of the adhesive composite section as explained below.

(i) *For Slip Level I:* $\lambda \le \lambda_o$

Since slip is independent of the state of the cross-section, at any slip level, the adhesive composite section could be in any of the abovementioned states. The governing equation can be solved for each state, subject to the $\lambda \le \lambda_o$ constraint or as shown below.

Considering Eq. (11) and Eq (4) and the shear-slip relationship in Eq. 12, the second-order differential equation can be obtained:

$\frac{d^2 F_a}{dz^2} - \omega_\alpha^2 F_a = -\eta_\alpha$	(13)

with

$\omega_\alpha^2 = \alpha b_a \left(\mu^* + k^* d_s\right)$	(14a)
$\eta_\alpha = \alpha b_a \left[\left(M_e + m^*\right)k^* - n^*\right]$	(14b)

The generic solution of the second-order differential equation is calculated:

$F_a(x) = c_1 e^{\omega_a x} + c_2 e^{-\omega_a x} + \frac{\eta_\alpha}{\omega_\alpha^2}$	(15)

(ii) *For Slip Level II:* $\lambda > \lambda_o$

For slip level II, a second-order differential equation similar to Eq. (123) can be written as

$\frac{d^2 F_a}{dz^2} + F_a \omega_\beta^2 = \eta_\beta$	(16)

with

$\omega_\beta^2 = \beta b_a \left(\mu^* + k^* d_s\right)$	(17a)
$\eta_\beta = \beta b_a \left[\left(M_e + m^*\right)k^* - n^*\right]$	(18b)

The generic solution of the second-order equation is reported in Eq. 19

$F_a(x) = c_3 \sin(\omega_\beta x) + c_4 \cos(\omega_\beta x) + \frac{\eta_\beta}{\omega_\beta^2}$	(19)

The external moment for the case considered is expressed in Eq. 20. It is important to underline that different loads can be applied in the current analytical model, changing the expression of Eq. 20.

$M_e = \frac{qb_a\left(\frac{L_q^2}{2} - x^2\right)}{4}$	(20)

Furthermore, the integration constants c can be evaluated based on the boundary conditions of the connection:

$\frac{dF_a}{dx}(0) = 0$	(21a)
$\frac{d^2F_a}{dx^2}\left(\frac{L}{2}\right) = 0$	(21b)

2.2 *Numerical Solution Scheme*

The connection is divided into several finite segments and since the problem is nonlinear, the load is applied incrementally. Initially, all the segments will have zero slip (slip level I), thus the solution would be based on the elastic branch of cohesive law. Once a segment is entered in the softening branch the appropriate analytical solution needs to be applied. At the common point of adjoining segments x_i and x_{i+1}, the following continuity conditions must be satisfied:

$F_{ai,j}(x_i) = F_{i,j}(x_{i+1})$ (continuity of shear force)	(22a)
$\frac{dF_{ai,j}(x_i)}{dx} = \frac{dF_{ai,j}(x_{i+1})}{dx}$ (continuity of strain)	(22b)

Due to the nonlinear nature of the problem, the solution must be iteratively performed, and the iteration will be terminated once a pre-selected convergence criterion is satisfied. In the present analysis, at the transition points of the adhesive connection from one stress state to another, it is checked to make sure that the steel adherent moment corresponds to M_{sy} (at the transition from State 1 to 2).

Finally, at a common point of each two adjoining segments, the slip exhibited at the interface between the two adherents is controlled ($\lambda < \lambda_0$ or $\lambda > \lambda_0$).

3. Experimental tests

To characterize the mechanical properties of the adhesive interface exposed to short ageing conditions, double lap shear and end notched flexure (ENF) specimens have been realized and tested at the Laboratory of Mechanics and Acoustic (LMA) in Marseille.

The double lap shear joints have been dimensioned following the geometrical configuration of Type B of ASTM Standards D 3528-96 [39]. In particular, each specimen has been constituted by four steel plates, two of dimensions 112x26x4 mm and the other two of 50x26x2 mm, respectively, bonded together by means of an adhesive layer of overlap length equal to 20 mm and a thickness of 4 mm as depicted in Figure 6. The perfect alignment of steel plates has been guaranteed by an aluminium device. To ensure perfect adhesion, the steel surface has been cleaned with acetone.

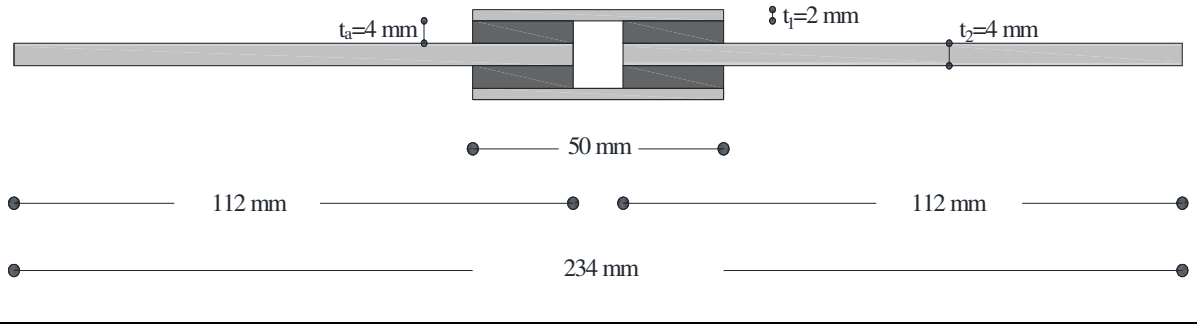

Figure 6. Double lap shear joints according to ASTM Standards D 3528-96

The geometrical dimensions of ENF tests have been fixed according to ASTM D7905/D7905M – 14 [40]. More in detail, two rectangular steel pieces of dimensions 240x15x15 mm have been bonding together with an initial pre-crack of 50 mm, as reported in Figure 7.

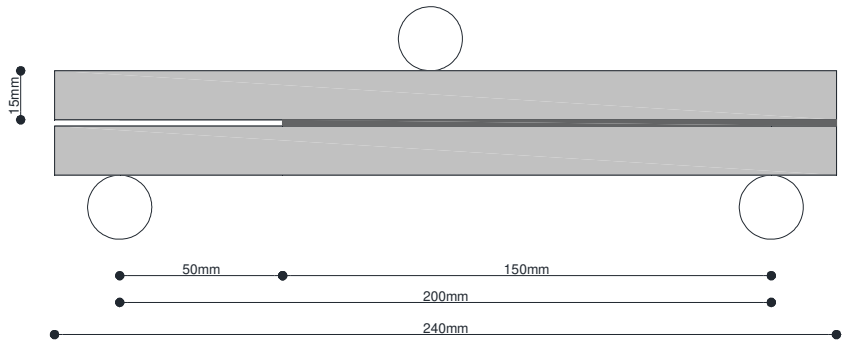

Figure 7 . ENF tests specimen geometry according to ASTM D7905/D7905M – 14

A total of 18 double lap shear joints and 10 ENF specimens have been fabricated. Some specimens are shown in Figure 8. The glue used in the current experimental investigation is a two-component polyurethane-based adhesive for structural bonding, containing no solvent and called Loctite UK 1351 B25 / Loctite UK 5452, available on the market. The mechanical properties declared by the produced [41] are reported in Table 1.

Table 1.Adhesive mechanical properties [41]

Mechanical Property	Unit	Value
Shear Strength, τ	MPa	20
Glass Transition temperature, T_g	°C	>70

The adhesive has been applied with a cartridge gun with a mixing of the two components. For both types of specimens S275 steel material has been used which mechanical properties are reported in Table 2.
Indeed, the environmental temperature if exceed the glass transition temperature (Tg) of the adhesive leads to relevant changes in its properties, determining, for instance, a transition from a hard to a rubbery behaviour, thus compromising its specific application [42].

Table 2. Steel S275 mechanical properties

Mechanical Property	Unit	Value
Yield Stress, f_{sy}	MPa	275
Ultimate Stress, f_{su}	MPa	360
Young's Modulus, E_s	GPa	210
Shear Modulus, G_s	GPa	81
Poisson's ratio, ν	-	0.3

3.1 *Aging Condition*

After a curing time of 7 days, the specimens were completely immersed in tap water inside two vessels (Figure 8) and introduced in ovens with a constant temperature of 60 degrees for a total ageing time of 148 days. It is important to underline that the temperature chosen is lower than the glass transition temperature, T_g. Inside the ovens, the vessels were covered by Teflon sheets able to withstand high temperatures for avoiding the evaporation of water and ensure a complete immersion of samples (Figure 9).

(a)

(b)

Figure 8. Specimens immersed in tap water: (a) double lap shear specimens; (b) ENF specimens

Figure 9. Specimens introduced in the oven

After the ageing time, the samples were taken from ovens and observed. As it is possible to note from Figure 10, the samples present corrosive phenomena on the steel surface. After the experimental tests, another observation has been done to verify the presence of corrosion at the interface between adhesive and adherents.

(a) (b)

Figure 10. Specimens after ageing time: (a) double lap shear specimens; (b) ENF specimens

3.2 *Water absorption*

The moisture content, M_t, absorbed by the polyurethane adhesive of each specimen immersed in the water was evaluated in accordance with the EN ISO 62:2008 [44], measuring the weight of dry material before water exposure, W_0 , and after exposure W_t, as follows:

$Mt(\%) = \left(\frac{W_t - W_0}{W_0} \right) 100$	(23)

The absorption of water was monitored using a balance with high precisions. Each measure was taken at 24 h of intervals.

The water absorption in the polyurethane adhesive is shown in Fig.11. As expected, the rate of water absorption is high at the early stages and then subsequently decreases. After 15 days, the adhesive continues to incorporate water at a small rate. The absorption process is complete after 42 days as a consequence the curve ends with a plateau.

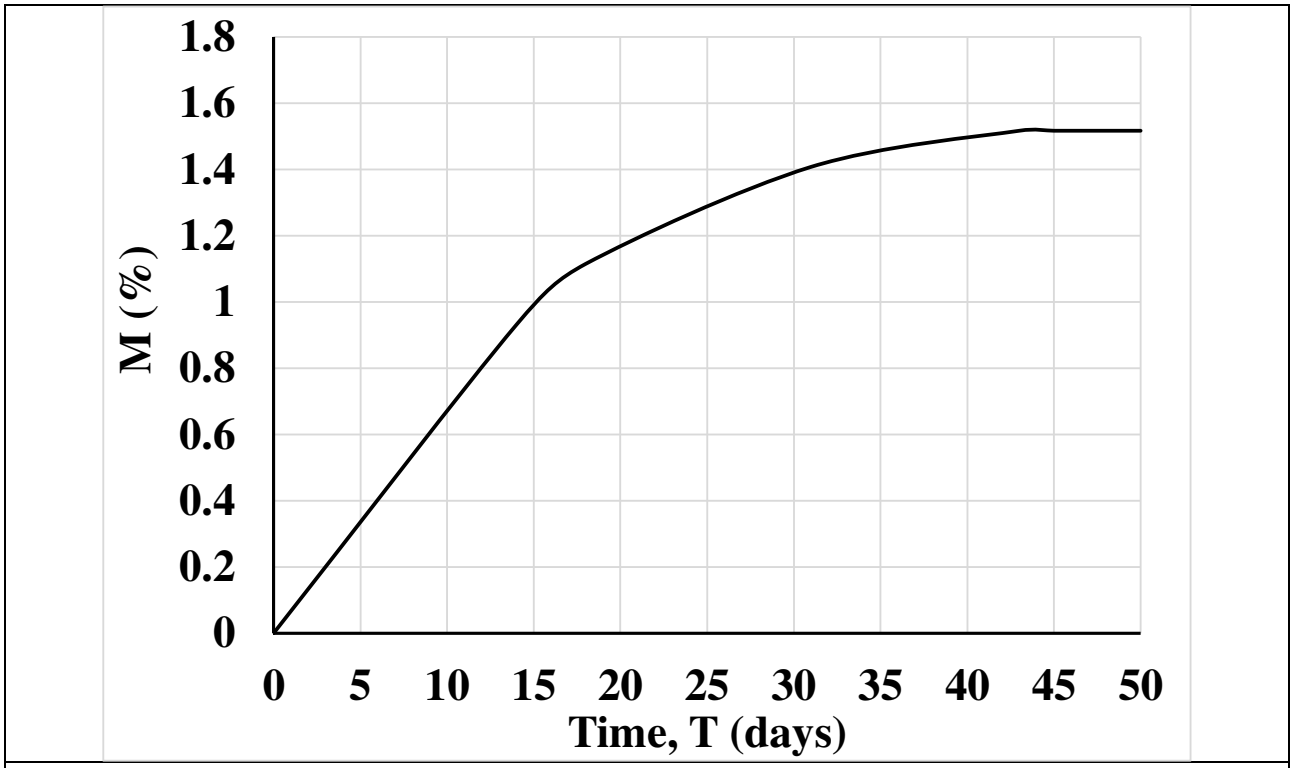

Figure 11 – Water absorption cure for polyurethane adhesive immersed in water

3.3 *Experimental Tests*

In this section, the two types of experimental tests, double lap shear joint and end flexural notched tests, are described, and analyzed in order to evaluate the mechanical properties of a polyurethane adhesive under hygro-thermal ageing.

(i) *Double lap shear joints Tests*

The double lap shear joints have been fixed at their ends in the grabs of the servo-hydraulic testing machine named “MTS 322 test frame” with a load capacity of 100 kN. The tests were carried out in displacement control at a rate of 1 mm/min (Figure 12) until to reach failure.

Figure 12. Double lap shear joints

The tests were performed with specimens characterized by the presence or the absence of short ageing conditions.

Figure 13 shows a specimen brought at failure after immersion in water. As it is possible to note, no corrosion phenomena are started at the interface between adhesive and steel plate but only on the steel surface not affected by the bonding.

Figure 13. Double lap shear specimen after being tested.

(ii) *End Notched Flexure Tests*

The End Notched Flexure specimens have been placed in an appropriate device able to apply a vertical force by means of a three-point bending test as shown in Figure 14. All the tests were performed in displacement control at a rate of 1 mm/min.

Figure 14. End Notched Flexure Tests.

The samples were tested before and after ageing conditions. The experimental data were continuously recorded by appropriate instrumentations.

3.3 *Experimental Results*

In this section, the experimental data have been analyzed with the scope to define and calibrate the interface law in Mode II. Furthermore, the founded mechanical parameters are involved in the analytical model proposed by the authors.

As above aforementioned, 18 double lap shear joints and 10 ENF specimens have been tested under monotonic load up to failure. Among them, 3 DLSJ and 3 ENF samples have been tested without ageing conditions (time, *T*, equal to 0), the other specimens have been tested after the days declared in Table 3, considering that after 42 days the moisture absorption process is complete (see Figure 11).

Table 3. Experimental results of double lap shear tests

Days	Test #	F_u [kN]	$F_{u,m}$ [kN]	δ_u [mm]	$\delta_{u,m}$ [mm]	τ_{av} [MPa]	$\tau_{av,m}$
0	L0#1	10.54	10.91	0.27	0.24	10.14	10.49
	L0#2	10.64		0.21		10.23	
	L0#3	11.55		0.24		11.10	
42	L42#1	17.16	16.10	0.33	0.31	16.50	15.48
	L42#2	17.91		0.35		17.22	
	L42#3	13.85		0.27		13.32	
	L42#4	17.78		0.34		17.09	
	L42#5	13.80		0.26		13.27	

72	L72#1	11.66	14.07	0.22	0.27	11.21	13.53
	L72#2	16.49		0.31		15.85	
133	L133#1	10.18	11.30	0.19	0.22	9.79	10.87
	L133#2	9.53		0.18		9.17	
	L133#3	14.18		0.27		13.64	
148	L148#1	13.28	13.59	0.25	0.26	12.77	13.07
	L148#2	14.55		0.28		13.99	
	L148#3	14.99		0.29		14.41	
	L148#4	12.07		0.24		11.61	
	L148#5	13.06		0.26		12.56	

The experimental results in terms of mean ultimate force vs ageing time are summarized in Figure 15. As it is possible to note, at the beginning the high temperature influences the polymerization process, increasing the shear strength followed by the beginning of the degradation process.

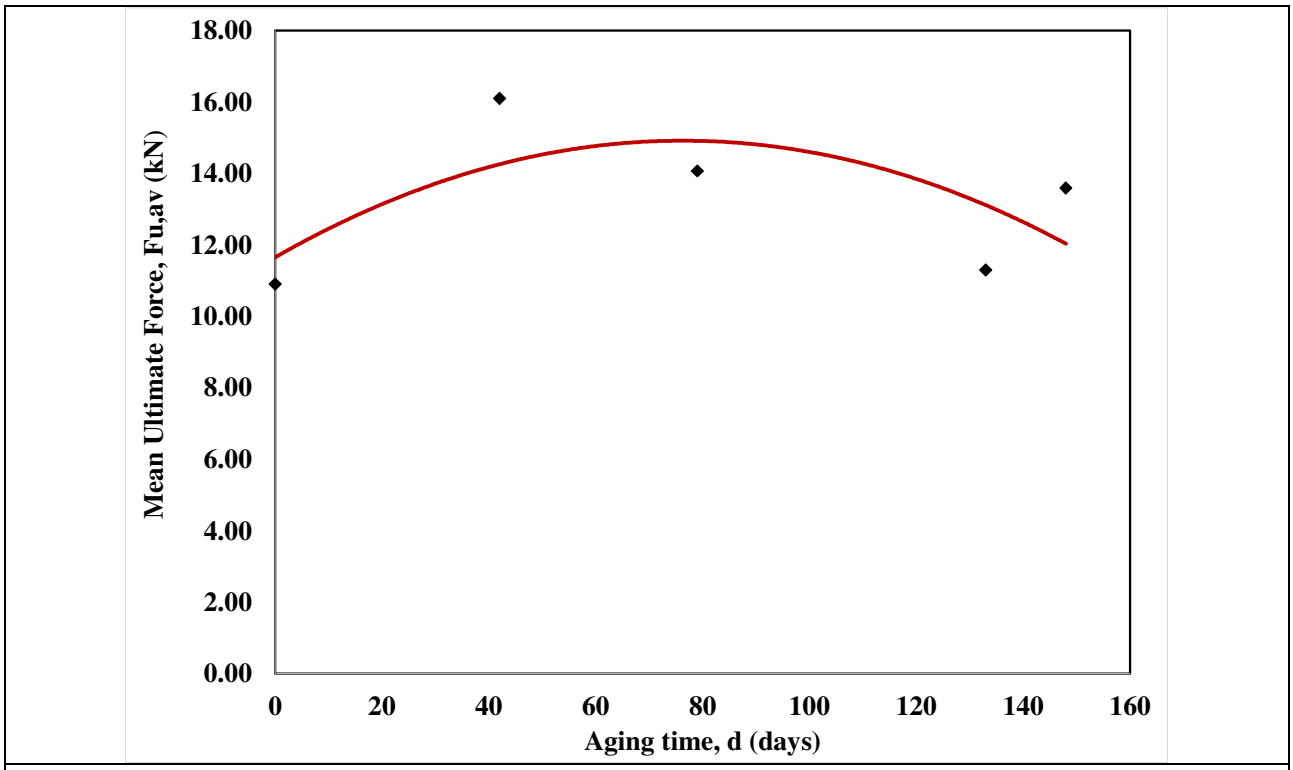

Figure 15. Variation of the ultimate force of double lap shear tests under the ageing condition

In Table 4, the evaluation of the energy fracture has been undertaken through the correct beam theory with effective crack method length (CBTE) [45], able to take into account the shear effects introduced in the specimen compliance. The CBTE is based on the equivalent crack estimation that does not need the measurement of debonding propagation and preliminary tests for adherend flexural modulus determination. With this approach, the critical strain energy release rate G_{II} is

$$G_{II} = \frac{9P^2a_e^2}{16B^2h^3E_L} \quad (23)$$

where $l=L/2$ is the half-span length, P is the applied load, a_e is the effective delamination length. The effective crack length, a function of elastic properties, can be easily obtained by Eq. 24:

$$a_e = \left[\frac{1}{3}\left(8C_c B h^3 E_L - 2l^3\right)\right]^{\left(\frac{1}{3}\right)} \quad (24)$$

where C_c is the corrected measured compliance.
Being the measured compliance Eq.25a equal to the ratio of tangential displacement to load, the corrected compliance is Eq.25b

$$C = \frac{\delta}{P} \quad (25a)$$

$$C_c = C - \frac{3l}{10GBh} \quad (25b)$$

where G is the shear modulus of steel adherends.

Table 4. Experimental results of ENF tests

Days	Test #	Fu [N]	δu [mm]	G_{II} [N/mm]
0	E0#1	4136	0.91	2.24
	E0#1	4928	0.97	2.82
	E0#1	4043	0.94	2.29
42	E42#1	8456	1.86	9.38
	E42#2	8066	1.70	8.18
72	E72#1	3943	0.85	2.42
	E72#2	-	-	-
148	E148#1	2335	0.61	0.85
	E148#4	3457	0.75	1.54
	E148#5	2728	0.64	1.04

3.3 *Evaluation of cohesive law.*

In this section, the cohesive law of the Loctite polyurethane adhesive is evaluated thanks to the experimental results obtained at different steps of ageing hygro-thermal condition due to the immersions of the adhesive in water at a constant temperature of 60°. The interface properties are defined also in the absence of ageing conditions.
As reported in the previous sub-sections the fracture energy in Mode II has been defined under short ageing conditions by means of the experimental data of ENF tests.
Using a bi-linear expression (see Eq. 12), by the knowledge of the energy of fracture and ultimate slip, it is possible to define the maximum shear stress reported in Table 5.
It is important to underline that the mean value of experimental tests has been considered in the current evaluations.

Table 5. Cohesive law parameter

Days	τ_m [N]	G [N/mm]	λu [mm]	λe [mm]
0	10.83	2.45	0.45	0.054
42	16.01	8.78	1.10	0.075
72	13.93	2.42	0.35	0.075
148	13.65	1.14	0.17	0.048

The parameters τ_m, λ_e and λ_u, are evaluated by reproducing the experimental results through the classical fundamental equation of double lap shear joint following the procedure described in Appendix A.

4. Numerical Analysis

4.1 *Validation of the analytical model*

To assess the robustness of the analytical model a comparison with the numerical results of a FEM model has been undertaken.
The structure considered (Figure 1) has the length of the first and second adherent equal to 1000 mm, and a thickness equal to 5 mm, on the other hand the length of the second adherent has a thickness equal to 20mm. For each adherent, the width is equal to 50 mm. Half part of the composite structure has been modelled due to the symmetry and appropriate boundary conditions have been set.
The properties of the adherents are reported in Table 2. To simulate the adhesive behaviour a bi-linear cohesive law has been introduced. The damage occurs only in the adhesive layer and its evolution is governed by energy in Mode II (GII) dissipated.
The properties of cohesive law are reported in Table 5 for the case characterized by the absence of ageing conditions.
A total of 13000 CPS4 (4-node bi-linear stress quadrilateral) elements with a length of 1 mm are used for meshing the adherents. Two numerical analyses have been performed for uniformly distributed loads equal to 0.162 and 0.280 N/mm^2, respectively (Figure 2).

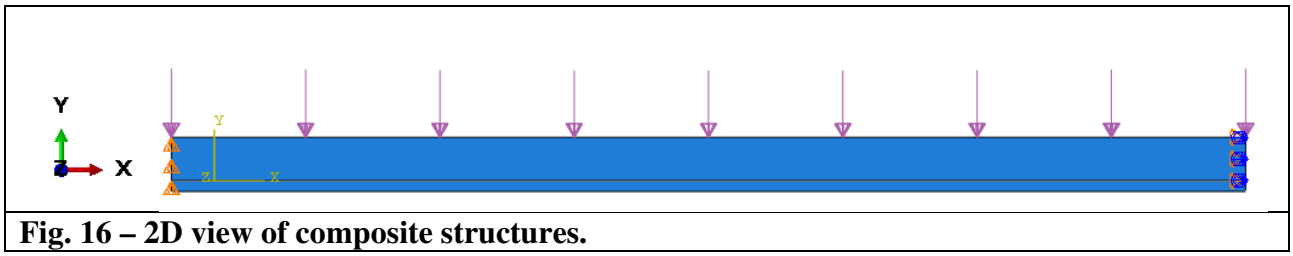

Fig. 16 – 2D view of composite structures.

Figure 16 shows a 2D view of the finite element model. The numerical results in terms of shear stress distribution along the adhesive layers are compared concerning the analytical one as depicted in Figure 17, for both uniform load levels.

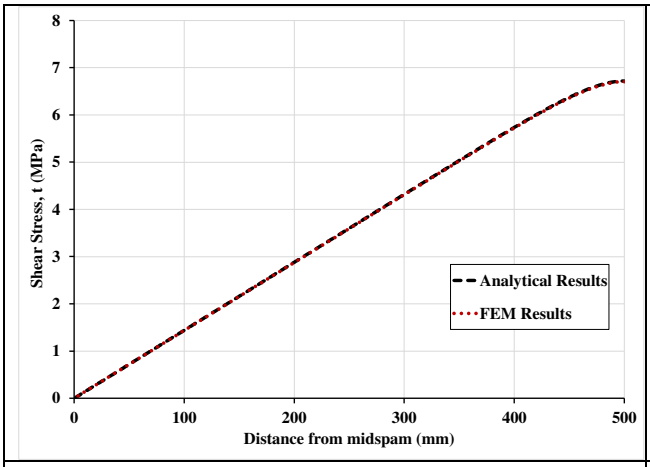

(a) 0.162

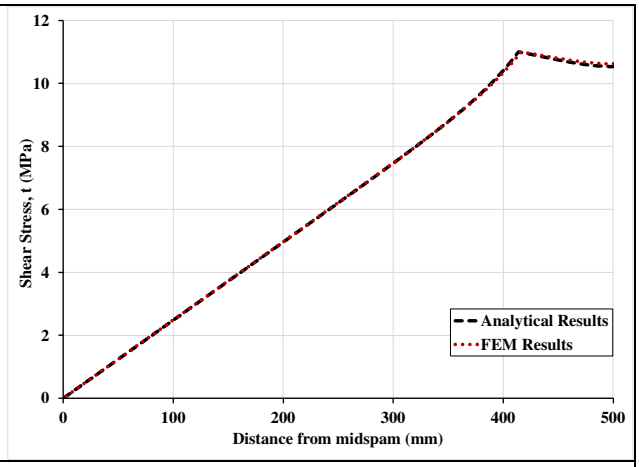

(b) 0.280

Fig. 17 – Shear stress distribution at the interface of adhesive connections: comparison between analytical and numerical data.

It is important to underline that the first load produce shear stress lower the elastic limit, on the other hand, the second load provoke slips higher the elastic limit in the external region of adhesive connections. As it is possible to note from Figure 15, the comparison between analytical and numerical data are in very good agreement showing the accuracy of the analytical procedure.

4.1 *Parametric analysis using the proposed model.*

A parametric analysis has been undertaken using the analytical formulations proposed. The model considers the cohesive lows of the polyurethane adhesive influenced by short ageing conditions due to the simultaneous presence of water and temperature.

The composite structure, the object of the parametric analysis, is characterized by a length, *Lq*, equal to 1000 mm, where the uniform load is applied, the width of each plate, *ba*, equal to 50 mm, the thickness of upper and lower plates, hs_1 and hs_2 equal to 20 and 5 mm, respectively.

The mechanical properties of adherents are reported in Table 2 while the mechanical properties of the interface layer are reported in Table 5.

Figure 18 shows the ratio between the ultimate uniform load at 42, 72 and 148 days and at time 0 (without ageing).

Figure 19 shows the distribution of shear stress at debonding load for any case analyzed while Figure 20 shows the corresponding slip.

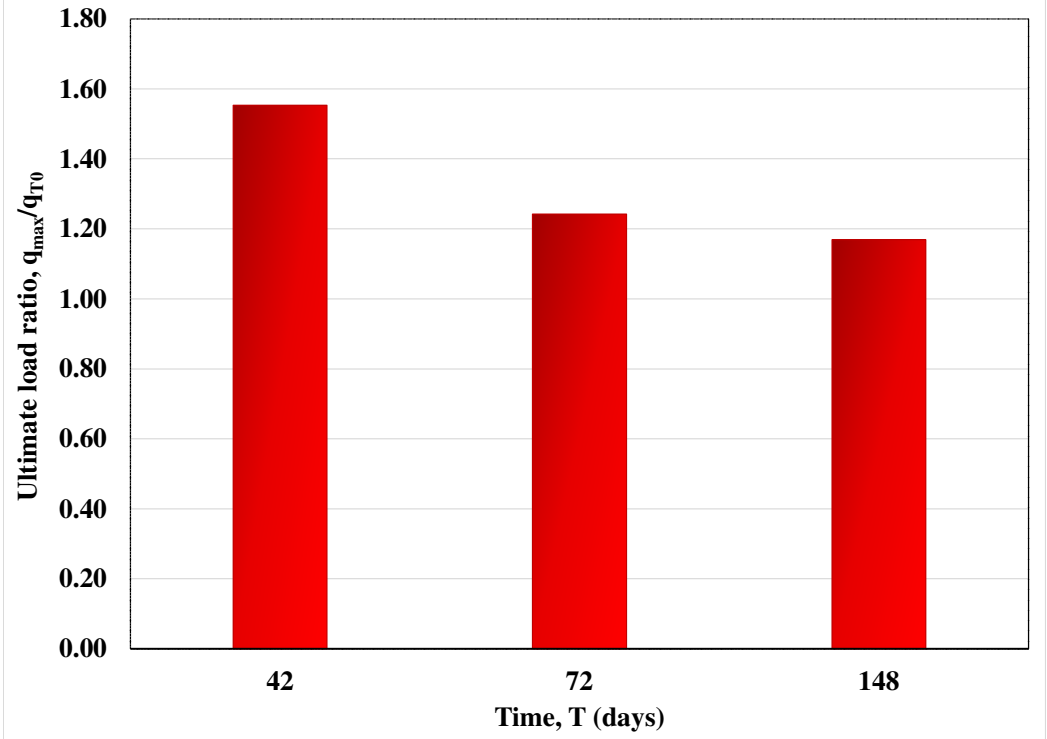

Figure 18 – Ultimate load ratio under short ageing

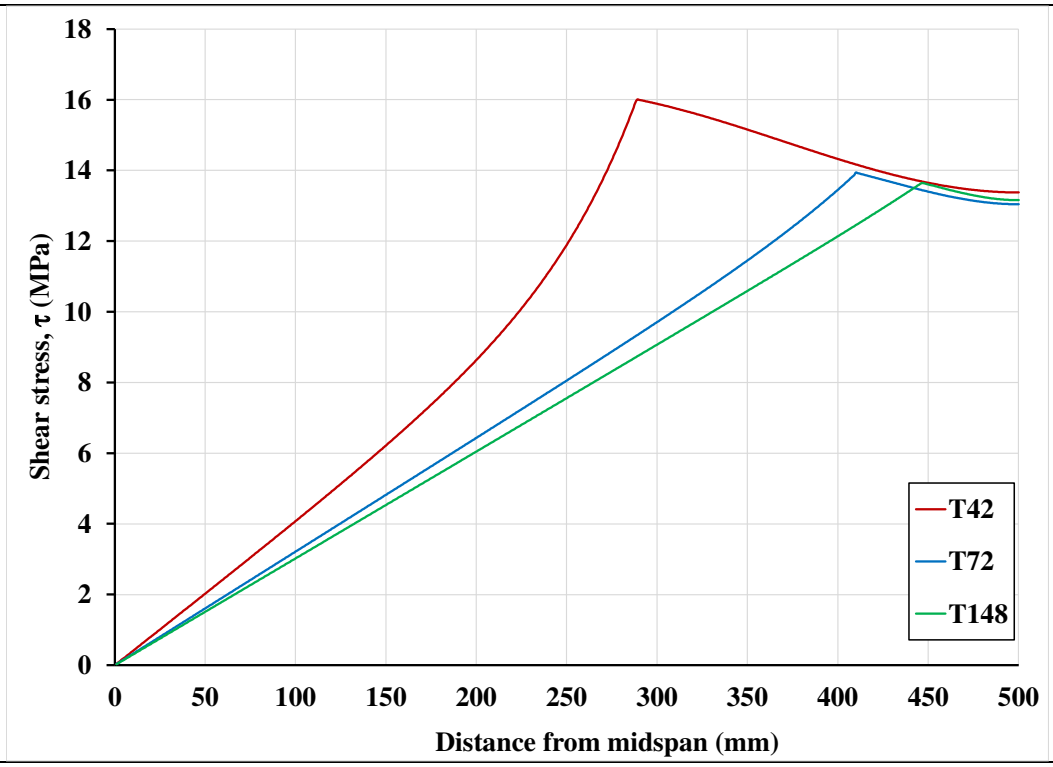

Figure 19 - Shear stress distribution at debonding along the adhesive length

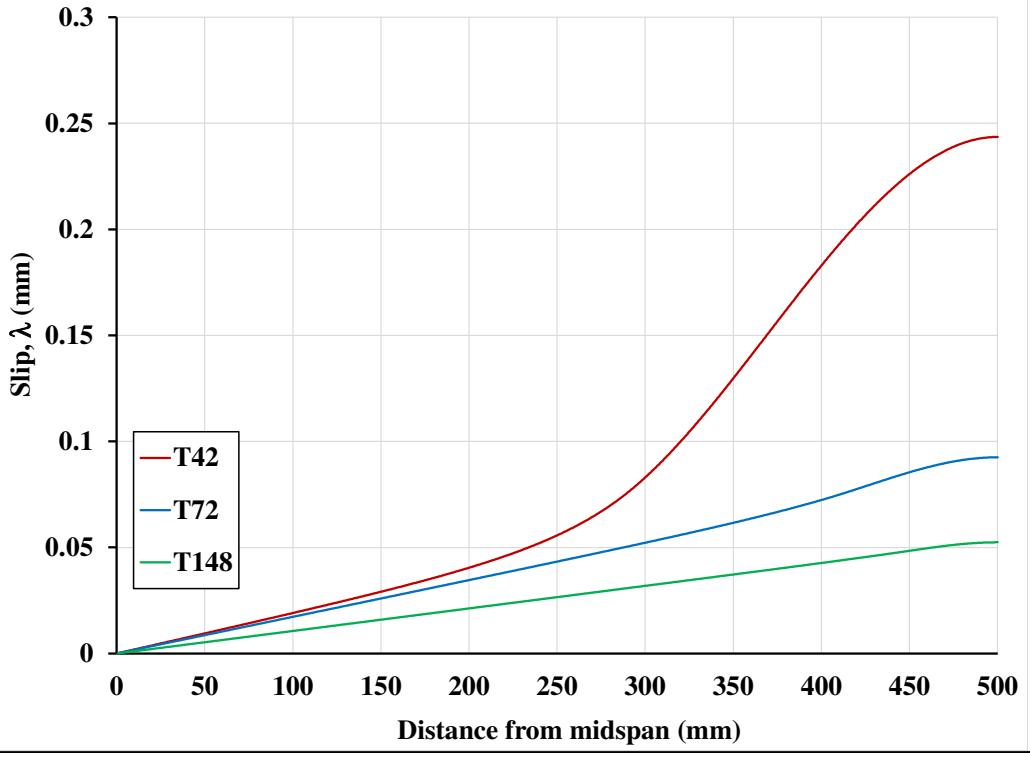

Figure 20 - Slip distribution at debonding along the adhesive length

As it is possible to note, the numerical results confirm the reduction of the ultimate uniform load and elevate aging time, shear stress and corresponding slip along the adhesive interface.

5. Conclusions

In this paper, a simple analytical procedure is proposed in order to study the behaviour of adhesive connections for secondary structures in marine environments. The analytical equations are based on Bernoulli beam theory taking into account the degradation of mechanical properties of the adhesive interface due to short ageing conditions. Double lap shear and End Notched Flexural tests have been performed to calibrate the properties of polyurethane adhesive under the combinate effects of water and temperature.

The numerical and experimental results support the following conclusions:

1) The analytical model has been validated thanks to the use of a fem model. The equations can take into account the non-linearity of adherents and adhesive, and the effects of ageing conditions.
2) The experimental results showed a reduction of polyurethane adhesive properties due to the effects of short ageing conditions.
3) The immersion of water produces corrosion phenomena on the external side of steel connections. No corrosion was observed at the interface between adherents and adhesive.
4) The model is proposed as a simple and useful instrument to design the secondary structure in marine environments.

Acknowledgements

This project has received funding from the European Union Horizon 2020 research and innovation programme under the Marie Sklodowska-Curie grant agreement No 843218-ASSO (Adhesive connection for Secondary Structures in Offshore wind installations).
The authors would also like to thank BW Ideol for its financial support.

References

[1] Kwon J S, Choi D G, Park J S, Lee Y S. Adhesive bonded composite laminate double lap joint and progressive failure analysis. ECCM – 18th European Conference on Composite Materials, June 2018.
[2] Saleh M N, Saeedifar M, Zarouchas D, De Freitas S T. Stress analysis of double-lap bi-material joints bonded with thick adhesive. International Journal of Adhesion & Adhesives 2020;ì, 97: 102480.
[3] Maurel-Pantel A, Lamberti M, Raffa ML, Suarez C, Ascione F, Lebon F. Modelling of a GFRP adhesive connection by an imperfect soft interface model with initial damage. Composite Structures 2020: 239; 112034
[4] Lamberti M, Maurel-Pantel A, Lebon F, Ascione F. Cyclic behaviour modelling of GFRP adhesive connections by an imperfect soft interface model with damage evolution. Composite Structures 2022, 279: 114741.
[5] Lamberti M, Maurel-Pantel A, Lebon F. Experimental characterization and modelling of adhesive bonded joints under static and non-monotonic fracture loading in the mode II regime. International Journal of Adhesion & Adhesives 2023: 124; 103394.
[6] Galvez P, Abenojar J, Martinez M A. Durability of steel-CFRP structural adhesive joints with polyurethane adhesives. Composites Part B 2019; 165: 1–9.
[7] Chattopadhyay DK, Raju KVSN. Structural engineering of polyurethane coatings for high performance applications. Prog Polym Sci 2007;32:352–418.
[8] Alia C, Arenas JM, Suarez JC, Pinilla P. Mechanical behavior of polyurethane adhesive joints used in laminated materials for marine structures. Ocean Eng 2016;113:64–74.
[9] Adam M, Lühring A, Popp M, Fecht S, Vallée T. Pre-applicable structural adhesives for timber engineering: glued-in G-FRP rods. Int J Adhesion Adhes 2016;67:121–7.
[10] Zain NM, Roslin EN, Ahmad S. Preliminary study on bio-based polyurethane adhesive/aluminum laminated composites for automotive applications. Int J Adhesion Adhes 2016;71:1–9.
[11] Liu S, Cheng X, Zhang Q, Zhang J, Bao J, Guo X. An investigation of hygrothermal effects on adhesive materials and double lap shear joints of CFRP composite laminates. Composites Part B 2016; 91: 431e440.
[12] Heshmati M, Haghani R, Al-Emrani M. Durability of bonded FRP-to-steel joints: effects of moisture, de-icing salt solution, temperature and FRP type. Comp B Eng 2017;119:153-167.
[13] Heshmati M, Haghani R, Al-Emrani M. Environmental durability of adhesively bonded FRP/steel joints in civil engineering applications: state of the art. Compos Part B-Eng 2015; 81: 259-75.
[14] Avendano R, Carbas RJC, Marques EAS, da Silva LFM, Fernandes AA. Effect of temperature and strain rate on single lap joints with dissimilar lightweight adherends bonded with an acrylic adhesive. Compos Struct 2016; 152: 34-44.

[15] Chamochin R, Cano de Santayana M, Abenojar J, Pantoja M, Ballesteros Y, del Real JC. The effect of surface treatment on the behavior of toughened acrylic adhesive/GRP (epoxy) composite joints. J Adhes Sci Technol 2010; 24: 1903-1916.
[16] Viana G, Costa M, Banea MD, da Silva LFM. A review on the temperature and moisture degradation of adhesive joints. Proc IMechE Part L: J. Materials: Design and Applications 2016; 0(0): 1-14.
[17] Korta J, Mlyniec A, Uhl T. Experimental and numerical study on the effect of humidity temperature cycling on structural multi-material adhesive joints. Compos Part B-Eng 2015; 79: 621-30.
[18] Agarwal A, Foster SJ, Hamed E. Testing of new adhesive and CFRP laminate for Steel- CFRP joints under sustained loading and temperature cycles. Compos Part B-Eng 2016; 99: 235-47.
[19] Costa M, Viana G, da Silva LFM, Campilho RDSG. Effect of humidity on the fatigue behaviour of adhesively bonded aluminium joints. Lat Am J Solids Stru 2017; 14: 174- 87.
[20] Heshmati M, Haghani R, Al-Emrani M. Durability of bonded FRP-to-steel joints: Effects of moisture, deicing salt solution, temperature and FRP type. Compos Part B-Eng 2017; 119: 153-67.
[21] Cognard P. Handbook of Adhesives and Sealants. Elsevier Science, 2005.
[22] Galvez P, Abenojar J, Martinez MA, Durability of steel-CFRP structural adhesive joints with polyurethane adhesives, Composites Part B 2018; 165: 1-9.
[23] Karbhari VM. Durability of Composites for Civil Structural Applications. Boca Raton, Florida: Woodhead publishing; 2007.
[24] Budzik MK, Jumel J, Salem NB, Shanahan MER. Instrumented end notched flexure – Crack propagation and process zonemonitoring Part II: Data reduction and experimental. Int J Solid Struct 2013;50:310–9.
[25] Campilho RDSG, de Moura MFSF, Ramantani DA, Morais JJL, Domingues JJMS. Buckling Behaviour of Carbon-Epoxy Adhesively-Bonded Scarf Repairs. J Adhes Scien Tech 2009;23:1493–513.
[26] Franklin VA. Christopher T. Fracture Energy Estimation of DCB Specimens Made of Glass/Epoxy: An Experimental Study. Adv Mat Scienc Eng; 2013. p. 412601.
[27] Viana G, Costa M, Banea MD, da Silva LFM. Behaviour of environmentally degraded epoxy adhesives as a function of temperature. J Adhesion 2017;93:95–112.
[28] Gupta VB, Drzal LT, Lee CYC, Rich MJ. The temperature-dependence of some mechanical properties of a cured epoxy resin system. Polym Eng Sci 1985;25:812–23.
[29] Firmo JP, Roquette MG, Correia JR, Azevedo AS. Influence of elevated temperatures on epoxy adhesive used in CFRP strengthening systems for civil engineering applications. Int J Adhes Adhes 2019;93:8–18.
[30] Barra G, Vertuccio L, Vietri U, Naddeo C, Hadavinia H, Guadagno L. Toughening of Epoxy Adhesives by Combined Interaction of Carbon Nanotubes and Silsesquioxanes. Mat 2017;10:1131.
[31] Machado JJM, Marques EAS, Barbosa AQ, da Silva LFM. Effect of hygrothermal aging on the quasi-static behaviour of CFRP joints varying the overlap length. Compos Struct 2019;214:451–62.
[32] Sousa JM, Correia JR, Gonilha J, Cabral-Fonseca S, Firmo JP, Keller T. Durability of adhesively bonded joints between pultruded GFRP adherends under hygrothermal and natural ageing. Compos Part B 2019;158:475–88.
[33] Heshmati M, Haghani R, Al-Emrani M. Environmental durability of adhesively bonded FRP/steel joints in civil engineering applications: State of the art. Compos Part B 2015;81:259–75.
[34] Heshmati M, Haghani R, Al-Emrani M. Effects of moisture on the long-term performance of adhesively bonded FRP/steel joints used in bridges. Compos Part B 2016;92:447–62.

[35] Haghani R. Analysis of adhesive joints used to bond FRP laminates to steel members–A numerical and experimental study. Constr build mat 2010;23:2243–51.
[36] Lamberti M, Ascione F, Napoli A, Razaqpur Ghani, Realfonzo R. Nonlinear Analytical Procedure for Predicting Debonding of Laminate from Substrate Subjected to Monotonic or Cyclic Load. Materials 2022; 15: 8690.
[37] Lamberti M, Maurel-Pantel A, Ascione F, Lebon F. Influence of web/flange reinforcement on the GFRP bonded beams mechanical response: A comparison with experimental results and a numerical prediction. Composite Structures 2016; 147: 247–259.
[38] Desai C K,Basu S Parameswaran V. Determination of Traction Separation Law for Interfacial Failure in Adhesive Joints at Different Loading Rates. Journal of Adhesion 2016; 92: 819-839.
[39] ASTM D3528 – 96 (2002). Standard Test Method for Strength Properties of Double Lap Shear Adhesive Joints by Tension Loading; September 10, 1996.
[40] ASTM D7905/D7905M – 14. Standard Test Method for Determination of the Mode II Interlaminar Fracture Toughness of Unidirectional Fiber-Reinforced Polymer Matrix Composites. 2014.
[41] LOCTITE UK 1351 B25 / LOCTITE UK 5452. Henkel AG & Co. KGaA 40191 Düsseldorf, Germany.
[42] Michels J, Widmann R, Czaderski C, Allahvirdizadeh R, Motavalli M. Glass transition evaluation of commercially available epoxy resins used for civil engineering applications. Compos Part B Eng 2015;77:484–93.
[43] de Moura MFSF, de Morais AB. Equivalent crack based analyses of ENF and ELS tests. Eng Fract Mech. 2008;75(9): 2584-2596.
[44] EN ISO 62 :2008 : Plastic-determination of water absorption.
[45] Olave M, Vara I, Usabiaga H, Arexabaleta L, Lomov S V, Vandepitte D. Nesting effect on the mode II fracture toughness of woven laminates. Composite: Part A 2015; 74:174-184.

Appendix A

The procedure described in Appendix A is applied in order to evaluate the mechanical parameters of cohesive law in Mode II. The fundamental equation of a double lap adhesive joint has been considered. The differential equations of the slip in the elastic and softening branch of cohesive law are reported in the following:

$\frac{d^2\lambda}{dz^2} - \omega_{\alpha,II}\lambda = 0 \text{ for } \lambda < \lambda_e$	(A.1)
$\frac{d^2(\lambda - \lambda_u)}{dz^2} - \omega_{\beta,II}(\lambda - \lambda_u) = 0 \text{ for } \lambda > \lambda_e$	(A.2)

with

$\omega_{\alpha,II}^2 = \frac{2b_a\alpha}{E_1A_1}$	(A.3a)
$\omega_{\beta,II}^2 = \frac{2b_a\beta}{E_1A_1}$	(A.3b)

The solutions assume the following expressions:

$\lambda(x) = A\cosh(\omega_\alpha z) + Bsenh(\omega_\alpha z)$	(A.4)
$\lambda(x) = \lambda_u + C\cos(\omega_\beta z) + Dsen(\omega_\beta z) \text{ for } \lambda > \lambda_e$	(A.5)

The differential equations have four integration constants, to find them it needs to impose appropriate boundary conditions: Continuity between equations A.4 and A.5, absence of slip in the centroid of the adhesive layer and the force applied.
For any case, the ultimate experimental force is applied as a boundary condition, the parameters $\tau_{m,}$ λ_e and λ_u are varying and the shear distribution in the adhesive layer is evaluated.
When the average value of numerical shear stress evaluated along the adhesive layer corresponds to the experimental one, the parameters $\tau_{m,}$ λ_e and λ_u are defined.

Appendix B.

Using the proposed model, the case depicted in Figure 1.b can be analyzed. The geometrical parameters are shown in Figure B.1.

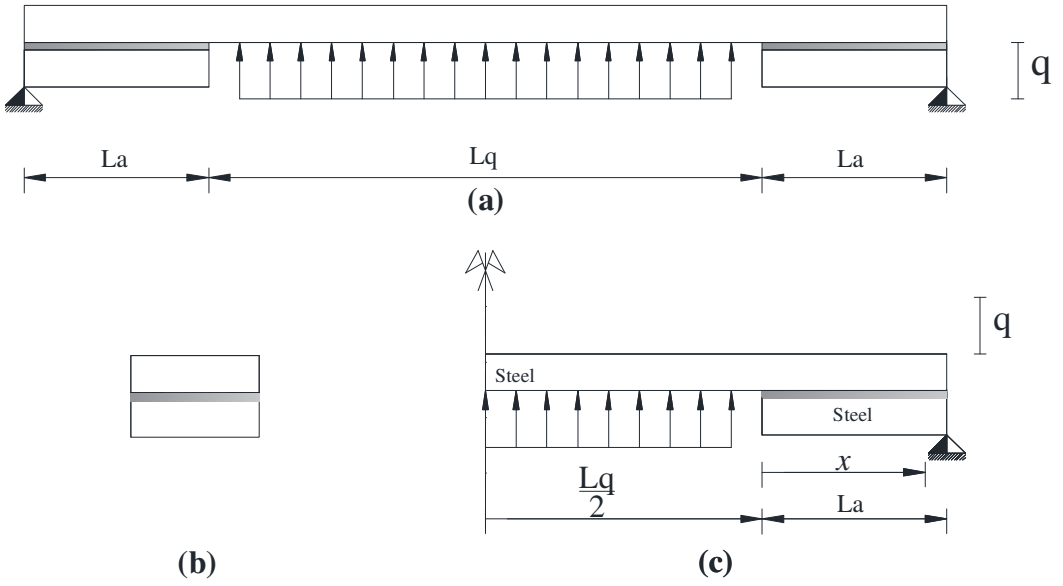

Figure B.1 - Composite beam (railing) analyzed.

Note in this case, only the adhesive connections of length La are considered. The results satisfy the Bernoulli beam theory when the height of adherent 1 and 2 is the same and the length La is higher than 10 times the height.

The composite structure considered is characterized by a length, *Lq*, where the uniform load is applied equally to 1000 mm, the half-length of adhesive connections, *La*, equal to 150mm, the width, *ba*, equal to 50 mm, and the thickness of each element, *hs*, equal to 5mm.

The analysis using the proposed model has been performed using the mechanical properties of the polyurethane adhesive defined experimentally under short ageing conditions. It is important to underline that ageing is due to the simultaneous presence of two boundary conditions: water and temperature. The mechanical properties of adherents are reported in Table 2 while the mechanical properties of the interface layer are reported in Table 5. The purpose of the parametric analysis is to demonstrate the variation of ultimate load applied at different days of aging conditions and the relative shear stress distribution.

Figure B.2 shows the ratio between the maximum uniform load applied before failure at 42, 72 and 148 days and the maximum uniform load at time 0.

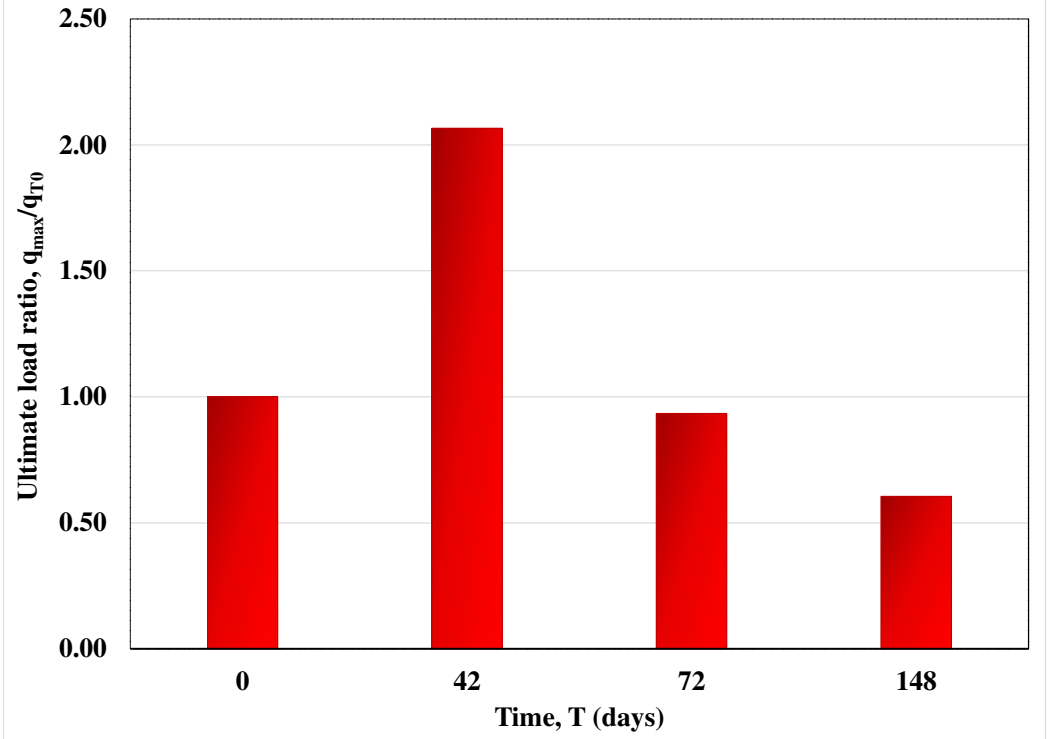

Figure B.2 – Ultimate load ratio under short ageing

The distribution of shear stress for any case is reported in Figure B.3.

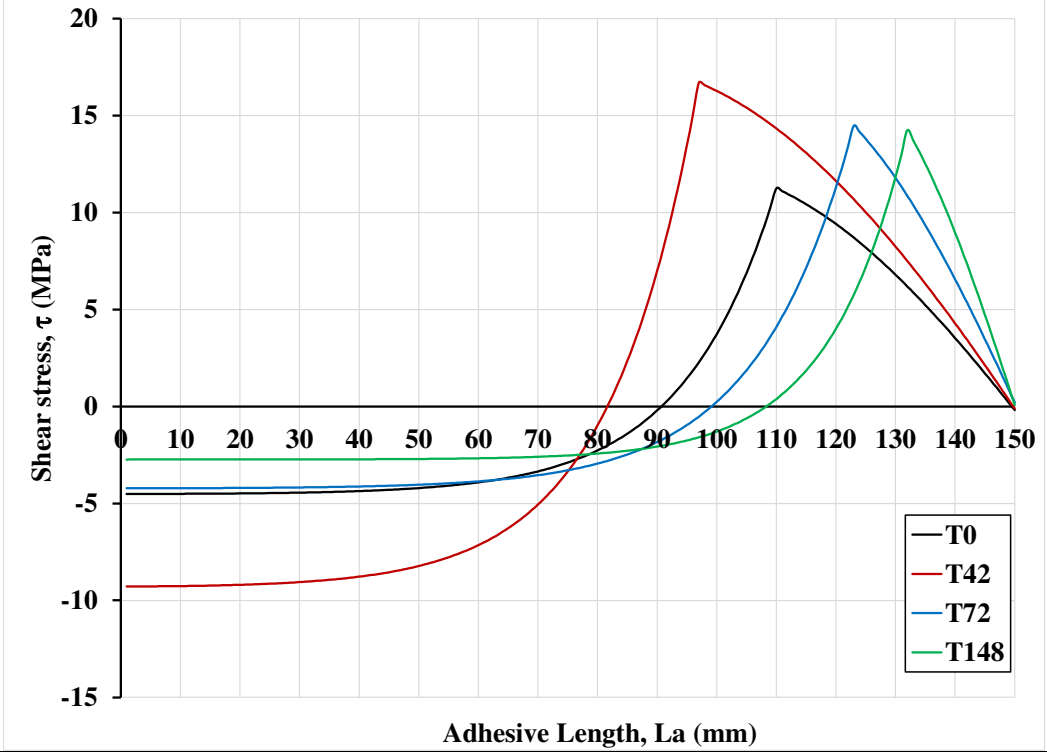

Figure B.3 - Shear stress distribution at debonding along the adhesive length